processes

MDPI

Article

Performance Optimization on 3D Diffuser of Volute Pump Using Kriging Model

Zhenhua Han [1], Wenjie Wang [1,2], Congbing Huang [3] and Ji Pei [1,*]

[1] Research Center of Fluid Machinery Engineering and Technology, Jiangsu University, Zhenjiang 212013, China; hansbox2022@163.com (Z.H.); wenjiewang@ujs.edu.cn (W.W.)
[2] Wenling Research Institute of Fluid Machinery, Jiangsu University, Taizhou 317522, China
[3] Jiangsu Aerospace Hydraulic Equipment Co., Ltd., Yangzhou 225699, China; jsgyhcb@126.com
* Correspondence: jpei@ujs.edu.cn

Abstract: In order to enhance the hydraulic performance of the volute pump, the Kriging model and genetic algorithm (GA) were used to optimize the 3D diffuser of the volute pump, and the hydraulic performance of the optimized model was compared and analyzed with the original model. The volute pump diffuser model was parameterized by BladeGen software. A total of 14 parameters such as the distance between the leading and trailing edges and the central axis, and the inlet and outlet vane angle were selected as design variables, and the efficiency under the design condition was taken as the optimization objective. A total of 70 sets of sample data were randomly selected in the design space to train and test the Kriging model. The optimal solution was obtained by GA. The shape and inner flow of the optimized diffuser were compared with those of the original diffuser. The research results showed that the Kriging model can effectively establish the high-precision mathematical function between the design variables and the optimization objective, and the R^2 value is 0.95356, which meets the engineering needs. The optimized geometry model demonstrated a significant change, the vane leading edge became thinner, and the wrap angle increased. After optimization, the hydraulic performance of the volute pump under design and part-load conditions were greatly improved, the efficiency under design conditions increased by 2.65%, and the head increased by 0.83 m. Furthermore, the inner flow condition improved, the large area of low-speed and vortex disappeared, the pressure distribution in the diffuser was more reasonable, and the pressure gradient variation decreased.

Keywords: volute pump; Kriging; surrogate model; CFD; 3D diffuser; optimization

Citation: Han, Z.; Wang, W.; Huang, C.; Pei, J. Performance Optimization on 3D Diffuser of Volute Pump Using Kriging Model. *Processes* **2022**, *10*, 1076. https://doi.org/10.3390/pr10061076

Academic Editor: Blaž Likozar

Received: 9 May 2022
Accepted: 25 May 2022
Published: 27 May 2022

1. Introduction

As a general machine, the pump assumes an important and fundamental function in modern production, and this is supported by the literature. Sakran et al. [1] systematically summarized the studies related to the effect of blade number on pump performance. Arun Shankar et al. [2] focused on the energy-saving effect of variable frequency drives (VFD) applied in pump systems. Liu et al. [3] summarized the published research results related to performance prediction and geometry optimization in pump-as-turbine. Al-Obaidi [4] used numerical methods to investigate the effect of different guide vanes on the flow field structure and axial pump performance under unsteady flow. Bai et al. [5] numerically investigated the effect of pressure fluctuations and unsteady flow patterns in the pump flow channel of three configurations with different numbers of diffuser vanes. Yang et al. [6] analyzed the fluid-dynamical analyses of unsteady flow in the first stage of a 12 multistage pump-turbine where hump instability occurs.

The hydraulic volute pump plays a key role as the core equipment in the high head, high flow, long-distance water-transfer project. At the same time, large-scale water transfer projects, as an important part of the national water infrastructure, also put forward higher

requirements for the performance of the volute pump. Among them, good operational stability and high operating efficiency is indispensable. The design of an efficient pump hydraulic model is heavily dependent on the engineering experience of the designer. For relatively inexperienced engineering designers, the optimal design of the hydraulic model is a key step in improving the efficiency of the model. Li et al. [7] summarized the common methods used in turbomachinery aerodynamics optimization, which are also commonly used in the field of pump hydraulic optimization and can be divided into three main categories: design of experiments (DOE), surrogate models, and intelligent algorithms. DOE mostly adopted Taguchi experimental designs by selecting enough representative points in the design space to analyze the influence of parameters on performance. Intelligent algorithms mainly included genetic algorithms (GA), particle swarm algorithms (PSO), gravitational search algorithms (GSA), etc., combined with the DOE method to seek the optimal solution directly in the design space. The main elements and advantages and disadvantages of each method are listed in Table 1.

Table 1. Comparison of the advantages and disadvantages of different optimization methods.

Methods	Contents	Advantages	Disadvantages
Design of experiments	Taguchi experimental design	Short optimization period, easy to obtain optimal solution	The design parameters are limited and the resulting solution is not optimal
Surrogate models	Artificial neural network Kriging model Response surface method	Short optimization period and low consumption of computational resources	There are errors between the surrogate model and the actual
Intelligent algorithms	Genetic algorithms Particle swarm algorithms Gravitational search algorithms	Multiple design parameters	Long optimization period and high consumption of computational resources

The surrogate model approach is a common method in modern optimization. Its main concept is to use an approximate mathematical model instead of a complex and time-consuming numerical computation process. Cho et al. [8] used an artificial neural network (ANN) model to optimize the operating conditions of a new explosive waste treatment method to reduce NOx emissions. Zhang et al. [9] established an effective optimization framework for aerodynamic shape design based on the multi-fidelity deep neural network (MFDNN) model, which can significantly improve optimization efficiency and outperform the single-fidelity method. The Kriging model is a common surrogate model and has also been studied by many scholars. Keshtegar et al. [10] compared the accuracy of four methods, Kriging, response surface method (RSM), multivariate adaptive regression (MARS), and M5 model tree (M5 Tree), in solar radiation estimation. The periodic Kriging model was found to be superior to the other three models. Ren et al. [11] proposed two active learning approaches combined Kriging and ANN models for reliability analysis, and the proposed methods can effectively assess, compared to a single typical surrogate model, the reliability of high and rare event problems with low computational cost. Hasanipanah et al. [12] investigated the accuracy and agreement of Kriging's nonlinear interpolation strategy for shear strength estimation at rock joints.

The application of the surrogate model approach in pump optimization design can effectively reduce the number of sampling points, shorten the computation time, and improve optimization efficiency. Tong et al. [13] compared the optimization prediction accuracy of the hydraulic loss model and three surrogate models for a ten-stage centrifugal pump and confirmed that the surrogate model was more accurate. De Donno et al. [14] proposed an open-source software-based surrogate optimization process to compare the effectiveness of Kriging and ANN models in pump optimization and validated it with an Ercoftac centrifugal pump. Ma et al. [15] used a machine-learning-based surrogate model to improve the hydraulic performance of a two-vane pump for wastewater treatment. Jaiswal et al. [16] selected the blade angle as the design variable, the shaft power, and

head as the optimization objectives, and used a hybrid surrogate model for multi-objective optimization of the centrifugal pump impeller. Chen et al. [17] proposed an inverse design and optimization method based on an adaptive proper orthogonal decomposition (APOD) hybrid model that reduces the cost of numerical computation and improves the accuracy of flow field prediction. Gan et al. [18] performed a multi-objective optimization of the inlet pipe of an inline pump based on genetic algorithm (GA) and ANN model to improve the inlet flow conditions of the inline pump.

As a key hydraulic component, the diffuser plays an important role in the volute pump. Posa et al. [19] investigated the effect of different operating conditions and different diffuser vane angles on pressure pulsation by large eddy simulation (LES). In a study by Yang et al. [20] for a large vertical centrifugal pump, matching optimization of the diffuser and volute had been performed using a variety of surrogate models to reduce the operating energy consumption, with the efficiency under the design conditions as the optimization objective. Lai et al. [21] studied the energy loss in a single-stage centrifugal pump for different diffuser outlet diameters. Wang et al. [22] experimentally investigated the influence of the clocking effect on the performance of centrifugal pumps. In the existing literature, there are relatively few studies on surrogate model optimization, specifically for the diffuser of volute pumps. Therefore, optimization of the volute pump diffuser using the surrogate model approach will facilitate further improvement of pump performance.

In this paper, a high-precision nonlinear mathematical function was established between the geometric parameters of the diffuser and the pump efficiency based on the Kriging model, and the optimal combination of parameters was obtained using an optimization-seeking algorithm. A comparative analysis of the hydraulic model performance, inner flow, and energy loss before and after optimization was conducted to explore the effect of different diffuser vane shapes on the performance of volute pumps.

2. Numerical Calculation of Hydraulic Model and Experimental Verification

2.1. Hydraulic Model

The pump model was a vertical single-stage single-suction with a diffuser volute centrifugal pump with design flow Q_d = 920 m^3/h, head H = 21 m, speed n = 1250 r/min, and specific speed n_s = 235. Where the specific speed was calculated from Equation (1).

$$n_s = \frac{3.65nQ_d^{1/2}}{H^{3/4}} \quad (1)$$

The 3D modeling of the computational domain including the inlet and outlet pipe was completed by UG NX software, as shown in Figure 1. The volute outlet was located at the side and the cross-section was circular. The number of impeller blades was Z_{im} = 6 and the number of diffuser vanes was Z_{di} = 8. The remaining design specifics are shown in Table 2.

Table 2. Design specifics of the volute pump.

Design Parameters	Symbol	Value
Impeller inlet diameter	D_j (mm)	270
Impeller outlet diameter	D_2 (mm)	360
Impeller outlet width	b_2 (mm)	70.5
Impeller inlet blade angle	β_1 (degree)	24
Impeller outlet blade angle	β_2 (degree)	22
Wrap angle of impeller blade	φ (degree)	136
Diffuser inlet diameter	D_3 (mm)	365
Diffuser outlet diameter	D_4 (mm)	505
Diffuser width	b_3 (mm)	72
Volute inlet width	b_5 (mm)	72
Volute base circle diameter	D_5 (mm)	440
Volute outlet diameter	D_6 (mm)	350

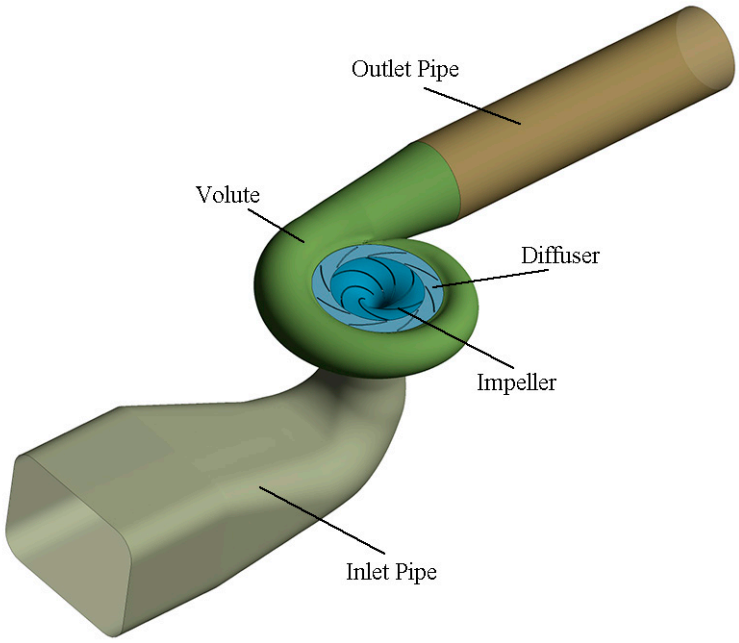

Figure 1. Computational domain of the volute pump.

2.2. Grid Sensitivity Analysis and Numerical Calculation

TurboGrid was used to build the impeller and diffuser mesh. Due to the complex structure of the volute, a hybrid mesh was generated for it with ICEM software, the key walls, such as the spacer tongue, were refined, and all walls were set with boundary layer meshes.

A total of 5 sets of independent meshes with element counts of 2.7 million, 5.02 million, 6.76 million, 9.6 million, and 11.7 million were generated. The results of efficiency and head calculation for the 5 sets of meshes are shown in Figure 2, in which the efficiency curve fluctuates, but the magnitude is not significant and the head curve does not increase significantly after the count of elements reaches 6.76 million. After comprehensive consideration, the third set of meshes was used for subsequent calculations. Part of the mesh is shown in Figure 3, and the number of elements in each domain is shown in Table 3.

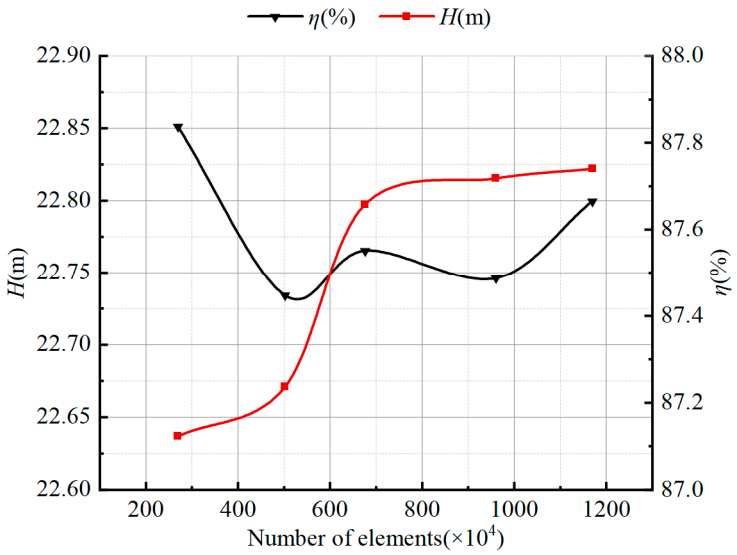

Figure 2. Results of grid sensitivity analysis.

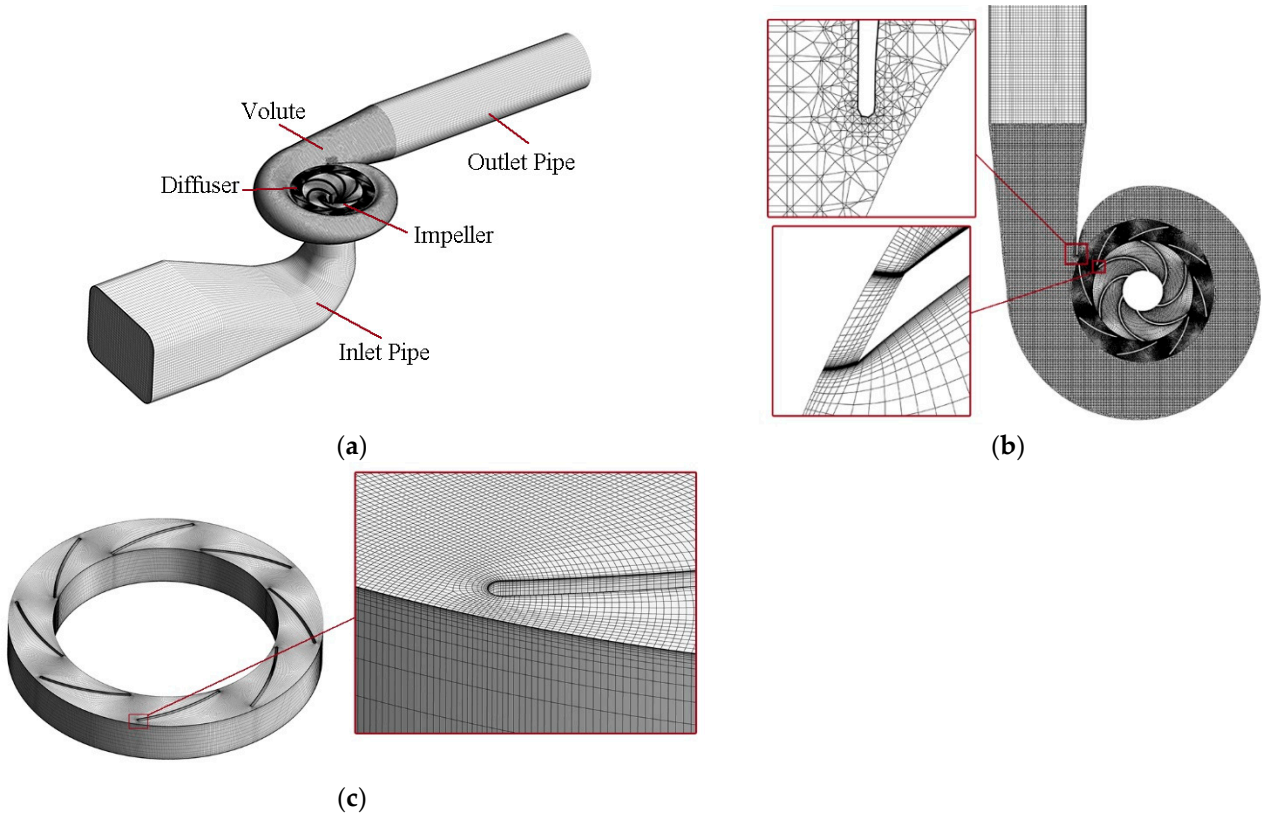

Figure 3. Mesh of the calculation domain: overall (**a**), the volute and impeller (**b**), the diffuser (**c**).

Table 3. Number of elements in each domain.

Domain	Number of Elements ($\times 10^4$)
Inlet pipe	36.5
Impeller	217.3
Diffuser	207.7
Volute	189.3
Outlet pipe	25.5

The numerical calculation of the pump model was performed using ANSYS CFX software, and the RNG k-ε turbulence model was used to close the N-S equations for solution. In the steady numerical calculation, the inlet boundary condition was the total pressure of 1 atm and the outlet boundary condition was the mass flow rate. The intersection between the impeller and the inlet pipe, and the impeller and the diffuser in the dynamic and static domain were set to Frozen rotor, and the wall was set to smooth. The convergence residual RMS was 10^{-5}, and the maximum number of computational iteration steps was 500.

2.3. Experimental Verification

The comparison of the performance curves obtained from the numerical calculation and the experimental results is shown in Figure 4. The trend of the calculated curve and the test curve was very similar; the calculated efficiency was 87.55% under the design condition and the test efficiency was 87.12%, with a difference of 0.43%. This indicates that the numerical calculation results were accurate.

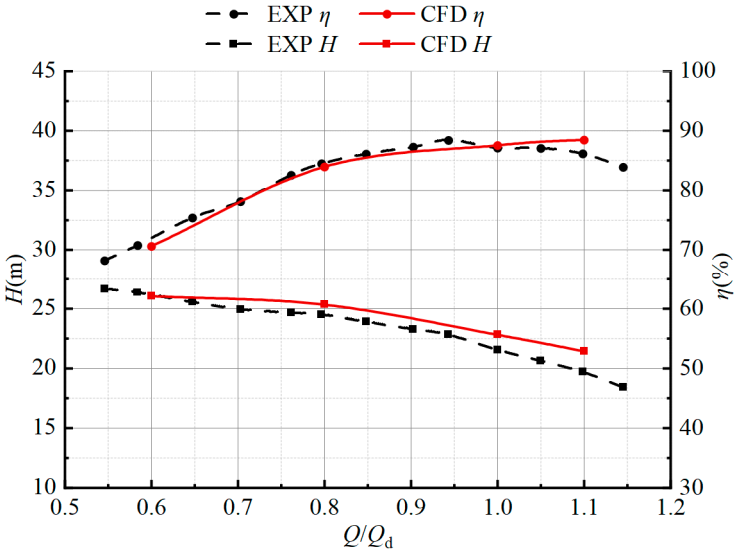

Figure 4. Comparison of calculated results with experimental results.

3. Optimization Process and Setting

3.1. The Kriging Model and Optimization Process

The Kriging model is an interpolation model which originated from geostatistics. The idea was first proposed by Krige [23], a South African mining engineer, in 1951, and then further promoted and applied by Professor Sacks et al. [24] in 1989. It has become a representative agent model in modern optimization methods. Its good ability to approximate nonlinear functions has allowed it to also be used in many applications in pump optimization design. The mathematical expression is shown as Equation (2).

$$y = \sum_{i=1}^{k} \beta_i f_i(x) + Z(x) \tag{2}$$

where $f_i(x)$ is the basis function of the regression model, β_i is the regression coefficient, and $Z(x)$ is a stationary stochastic process with mean 0 and covariance as follows:

$$Cov[Z(x_i), Z(x_j)] = \sigma^2 R(x_i, x_j) \tag{3}$$

where σ^2 is the variance of $Z(x)$, and $R(x_i, x_j)$ is the correlation function between x_i and x_j. In this paper, the Gaussian function was chosen as the correlation function.

The overall optimization process in this paper is shown in Figure 5. Firstly, the optimization objective, design variables, and their range were determined. Next, multiple sets of data were randomly selected from the design space and divided into two parts, one for model training and the other for model testing, without duplication between the two parts. In the next step, R^2 was calculated based on the training and testing results, and if it met the accuracy requirements, the optimal value of the model was found using the optimization-seeking algorithm and the data were recorded; otherwise, the data were sampled again to train the model. The above process was repeated several times, and finally, the optimal result was selected as the optimization result output, and the process was finished.

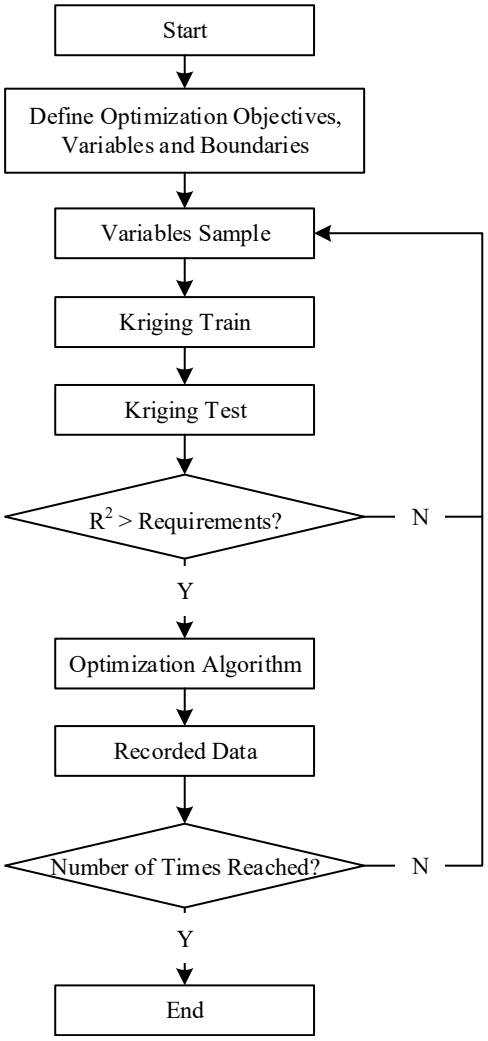

Figure 5. The process of optimization.

3.2. Optimization Objectives, Design Variables, and Ranges

Hydraulic efficiency is an important energy consumption characterization of the model. Obtaining an efficient hydraulic model, especially for design conditions, is the main goal of pump optimization design. In this paper, the maximum hydraulic efficiency of the model under the design conditions was taken as the optimization objective, which was calculated as follows:

$$\eta_{Q_d} = \frac{\rho g H Q_d}{T\omega} \tag{4}$$

where, T is the impeller torque, ω is the impeller angular velocity, H is the model head, and the calculation formula is

$$H = \frac{p_{2tot} - p_{1tot}}{\rho g} \tag{5}$$

where, p_{2tot} is the total pressure at the outlet of the pump, and p_{1tot} is total pressure at the inlet of the pump.

BladeGen was used to complete the parameterization of the diffuser model. In BladeGen, the vane angle curves in the hub plane and shroud plane were fitted with 4th-order Bessel curves to achieve parametric control of the diffuser vane geometry. According to engineering experience, the vane angle, as well as the leading and trailing edges, had a large impact on the performance. A total of 14 design variables, numbered x_0–x_{13}, were chosen to achieve fine control of the vane shape when combined with the BladeGen software

parametric modeling method. Among these variables, x_0 and x_1 were the distances from the intersection of the leading edge of the diffuser vane with the hub plane and the shroud plane to the central axis of the diffuser, respectively, and x_2 and x_3 were the distances from the intersection of the trailing edge of the diffuser vane with the hub plane and the shroud plane to the central axis of the diffuser, respectively, as shown in Figure 6a. Variables x_4–x_8 showed the y-coordinate values of the 5 Bezier curve control points in the hub plane, as shown in Figure 6b. Variables x_9–x_{13} showed the y-coordinate values of the 5 Bezier curve control points in the shroud plane, with the same graph as the hub plane. The x-coordinates of each Bessel curve control point were evenly distributed and fixed, and the upper and lower boundaries of each design variable are listed in Table 4.

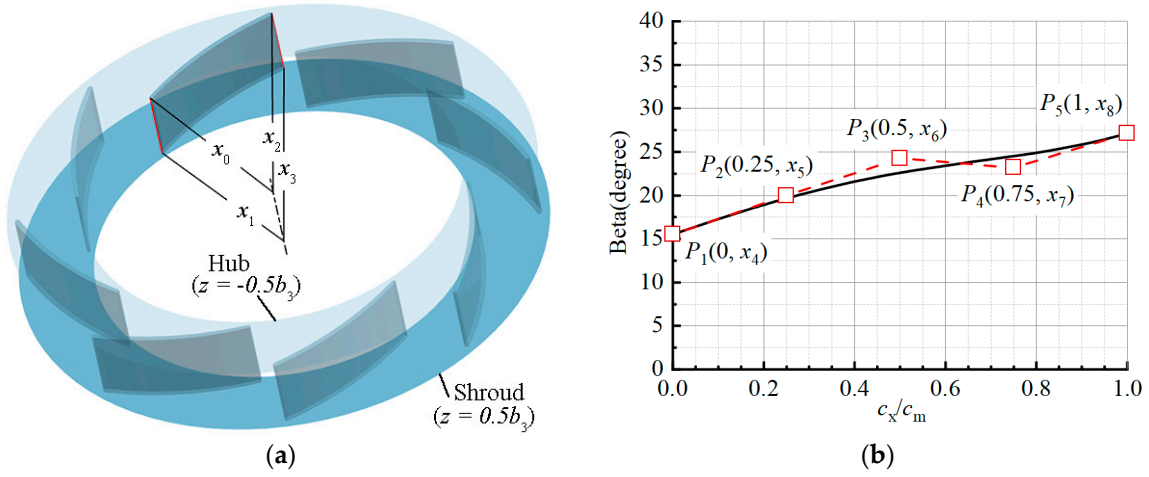

Figure 6. Schematic diagram of design variables: x_0–x_3 (**a**), x_4–x_8 (**b**).

Table 4. Design variable boundaries.

Variables	x_0	x_1	x_2	x_3	x_4	x_5	x_6	x_7	x_8	x_9	x_{10}	x_{11}	x_{12}	x_{13}
Upper Bound	0.19	0.19	0.252	0.252	30	40	40	40	30	30	40	40	40	30
Lower Bounds	0.184	0.184	0.242	0.242	15	10	10	10	22	15	10	10	10	22

3.3. Samples and Optimization of Process Parameter Setting

A total of 70 sets of data were randomly selected in the design space, of which the first 50 sets were used to train the Kriging model and the remaining 20 sets were used to test. All of them automatically called 3D modeling, meshing, and numerical calculation software to complete the numerical calculation to obtain the corresponding efficiency. Some of the data are listed in Table 5. The series of sampling, training, and testing processes were repeated a total of 50 times. The R^2 criterion was greater than or equal to 0.95. After the model was trained to the standard, the GA was used to find the best, and the number of populations of the algorithm was set to 80 and the number of iterations was set to 300.

Table 5. Partial sample data.

No.	1	2	3	4	5	...	66	67	68	69	70
x_0	0.1887	0.1863	0.1895	0.1875	0.1899	...	0.18708	0.18499	0.18587	0.18733	0.18673
x_1	0.1853	0.1869	0.1865	0.18743	0.1859	...	0.18681	0.1874	0.18775	0.18738	0.1873
x_2	0.2495	0.2515	0.24417	0.252	0.24883	...	0.2505	0.252	0.252	0.25117	0.24917
x_3	0.24417	0.25183	0.25083	0.24956	0.24683	...	0.252	0.24963	0.2487	0.252	0.25066
x_4	23.25	28.25	26.75	30	15.25	...	22.25	26.75	30	27.25	30
x_5	24.5	12.5	15.5	11.93	26.5	...	12.75	15.41	10.34	17.15	13

Table 5. *Cont.*

No.	1	2	3	4	5	...	66	67	68	69	70
x_6	35.5	14.5	12.5	11.5	22.5	...	26.5	14.5	10	11.3	18.5
x_7	34.5	10.5	26.5	10.5	30.5	...	13.5	21.5	10	18.5	10
x_8	22.4	22.13	25.33	24.5	26.13	...	22	25.73	23.73	23.31	23.66
x_9	28.75	19.25	15.25	22.75	17.75	...	22.25	20.25	21.29	21.44	19.5
x_{10}	26.5	28.5	21.5	14.76	19.5	...	26.75	20.91	21.37	25.13	21.79
x_{11}	10.5	26.5	14.5	17.43	25.5	...	29.52	24.86	16.5	21.76	18.96
x_{12}	29.5	15.5	37.5	17.22	19.5	...	16.64	14.82	15.99	21.5	13.53
x_{13}	24.27	29.87	29.33	28.26	23.73	...	29.07	27.32	26.8	28	28.27
η (%)	84.7	86.49	84.82	87.5	84.65	...	84.98	85.63	87.72	85.84	86.55

4. Discussion of Results

4.1. Surrogate Model Check and Comparison of Diffuser Vane Geometry

The R^2 analysis method was used to evaluate the prediction accuracy of the model. The evaluation results are shown in Figure 7. It can be seen that the predicted value had good consistency with the actual value, the prediction accuracy was high, and the R^2 value was 0.95356, which meets the engineering application standard. The R^2 calculation formula is as follows:

$$R^2 = 1 - \frac{\sum_{i=1}^{n} (\hat{y}_i - y_i)^2}{\sum_{i=1}^{n} (y_i - \overline{y})^2} \tag{6}$$

where $\hat{y}_i$ is the predicted value, y_i is the actual value, $\overline{y}$ is the average value, and n is the number of test points.

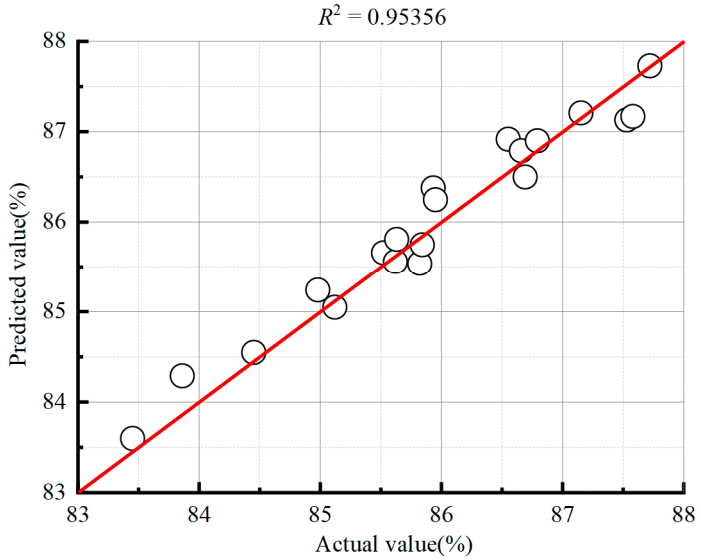

Figure 7. R^2 analysis of efficiency.

Table 6 shows the values of each design variable before and after optimization. All of them changed significantly except for x_4 and x_{12}. The vane inlet angle x_4 in the hub plane and the vane inlet angle x_9 in the shroud plane were no longer consistent. Meanwhile, the leading edge on the hub plane was closer to the center axis ($x_0 < x_1$) than on the shroud plane, indicating that the vane became twisted, which was also reflected in the optimized diffuser vane 3D model in Figure 8. The hub plane and the shroud plane vane outlet angle x_8, x_{13} was still relatively consistent. It can also be seen in Figure 8 that the hub plane and the shroud plane vane wrap angle were no longer the same, the shroud plane wrap angle was larger and the optimized model leading edge was thinner than the original model.

These changes resulted in less diffusion in the flow path between the diffuser vanes and a tighter inner flow.

Table 6. Comparison of design variables of diffuser.

Variables	x_0	x_1	x_2	x_3	x_4	x_5	x_6	x_7	x_8	x_9	x_{10}	x_{11}	x_{12}	x_{13}
Before	0.18774	0.18774	0.2484	0.2484	15.53	19.97	24.24	23.2	27.15	15.53	19.97	24.24	23.2	27.15
After	0.18426	0.18986	0.25171	0.25169	16.15	11.28	11.56	10.14	22.17	29.59	11.86	10.31	23.35	22.58

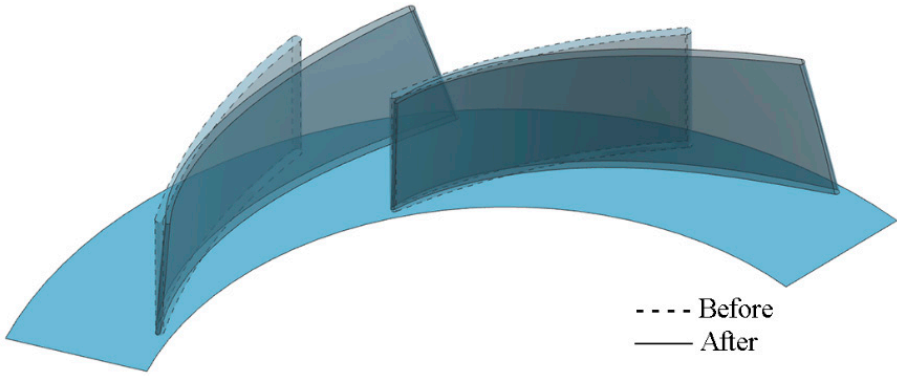

Figure 8. Comparison of 3D diffuser vanes.

4.2. Hydraulic Performance Curve Analysis

Figure 9 demonstrates the hydraulic performance curves of the optimized model compared with the original model in all working conditions. The efficiency under design conditions and part-load conditions was greatly improved. The efficiency was improved by 3.36% and 3.4% under 0.6 Q_d and 0.8 Q_d conditions, respectively, by 2.65% under design conditions, and the high efficiency area was widened. Meanwhile, the efficiency decreased under the over-load condition 1.1 Q_d, but only by 1.69%, so the efficiency of the optimized model can still be considered to have substantial improvement. Similarly, the model head also had a substantial increase under the design condition and part-load condition. Head under the design condition was increased by 0.83 m, while the high flow condition was slightly reduced. The model power decreased under the part-load condition and the design condition and over-load condition were consistent with the original model, indicating that the optimized model had better hydraulic performance and lower energy consumption, which ultimately achieved the goal of optimization.

4.3. Inner Flow Analysis

Figure 10 showed the velocity distribution and streamlines within the diffuser in different z-planes, respectively. For the convenience of description, the flow paths between the diffuser vanes were numbered from one to eight in a clockwise direction, respectively. It can be seen that the original model (Figure 10a) had a wide range of low-speed areas and vortex areas in the flow path, and these vortices blocked the flow path and seriously affected the performance. In the $z = -0.25\ b_3$ plane, the low-speed area was mainly distributed in the middle and outside of runners three and seven, outside of runner four, in most of runner eight, and there were also small low-speed areas outside of runner six. Most of these low-speed areas were near the back of the vane where the streamlines began to spread out and the flow separation phenomenon occurred. In runner eight, where the flow separation was most severe, the annular streamlines on the outside indicate that a vortex had developed in this area. The situation in the $z = 0$ plane was more severe, except for the runner five, which was good, the rest of the runners near the back side of the vane had a wide range of flow separation and vortex phenomenon. The streamlines on the outside of runners one and two turned at a large angle and extended along the outer circle of the

diffuser, indicating that the flow in the volute on the outside of the diffuser was also not optimistic. The $z = 0.25\ b_3$ plane was slightly better than the $z = 0$ plane, the streamlines in runners one and five were more satisfactory, while the rest of the runners also had flow separation and vortex phenomenon. These low-speed areas had a common feature, their locations were located in the runner near the back side of the vane.

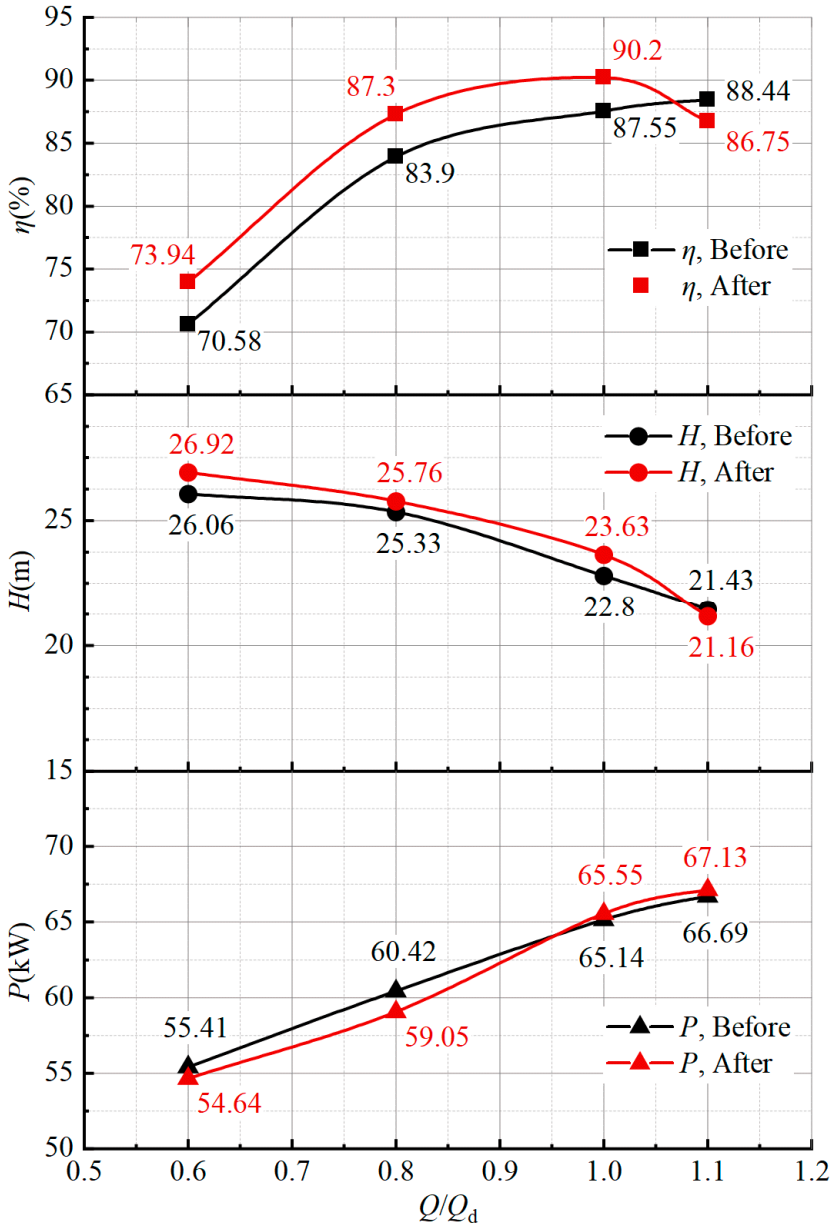

Figure 9. Comparison of hydraulic performance.

Compared to the original model, the streamlines between the diffuser vanes of the optimized model (Figure 10b) were improved significantly. The large low-speed area almost disappeared, only two vortices affecting three planes were outside of runners seven and three near the back of the vane, and a small low-speed area outside of runner four near the back of the vane also affected three planes. All other low-speed areas did not affect all planes and were small enough to have little effect on the streamlines. Overall, compared with the original model, the optimized model had a tighter streamline between the diffuser vanes, and there was no large range of low-speed areas blocking the flow paths. These inner flow changes resulted in improved hydraulic performance in the diffuser.

Figure 11 shows the pressure distribution in the diffuser in different z-planes. The pressure distribution between different planes was slightly different, but the difference was not significant. The pressure distribution grew gradually throughout the flow channel from inside to outside in the original model, with the blade working surface pressure being greater than the back, and the leading edge seeming high-pressure point due to direct fluid impact. Comparing the optimized model (Figure 11b) with the original model (Figure 11a), the pressure gradient variation in the diffuser of the optimized model was reduced, which was beneficial to pressure recovery and reduced energy loss. The point with high pressure disappeared because the vane leading edge became thinner and the intensity of direct impact by fluid was reduced.

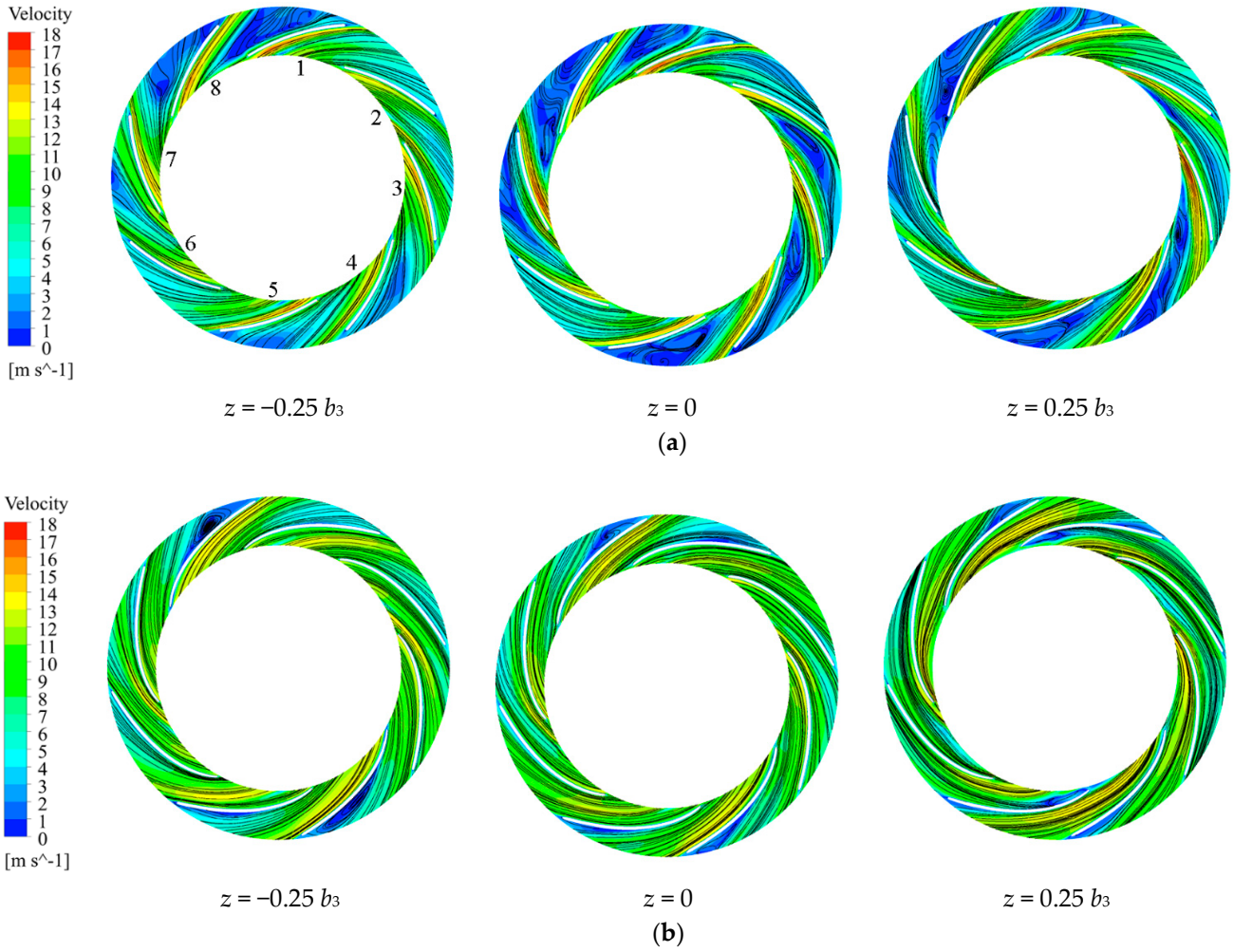

Figure 10. Comparison of different z-plane speeds and streamlines before (**a**) and after (**b**) optimization.

Based on the content of this paper, the collaborative optimization design of a hydraulic model for multiple operating conditions can be a further research direction to improve the current situation where the performance of the optimized model decreases under the over-load condition. Additionally, further research into the unsteady performance of the optimized model, considering the pressure fluctuation strength as the optimization objective to improve the operational stability of the volute pump, is recommended.

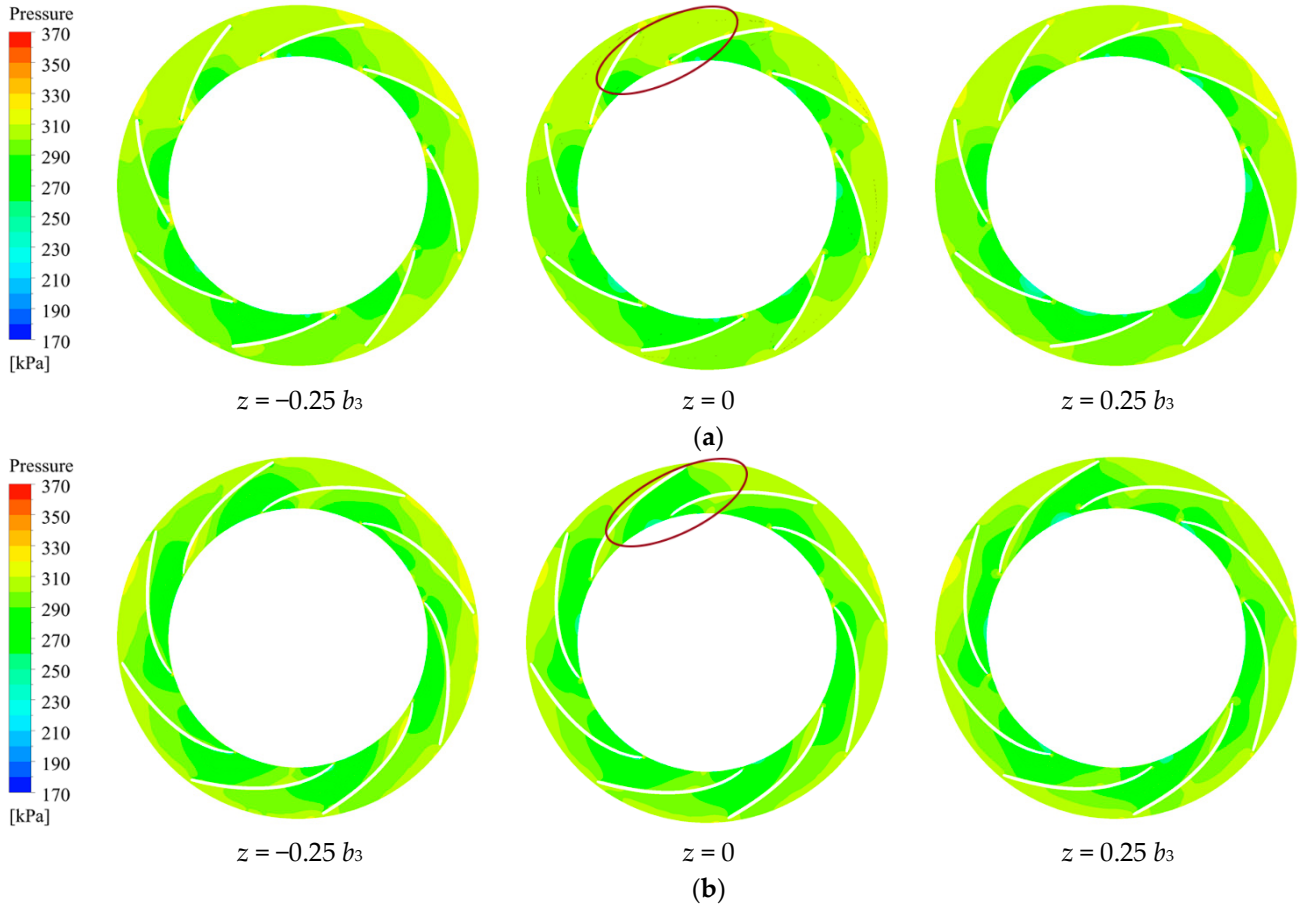

Figure 11. Comparison of different z-plane pressures before (**a**) and after (**b**) optimization.

5. Conclusions

In this paper, 14 parameters from the 3D diffuser of the volute pump were selected as design variables, and the model efficiency under design conditions was taken as the optimization objective. The diffuser was optimized based on the Kriging model and GA, and the hydraulic performance of the volute pump before and after optimization was compared and analyzed. The following conclusions were obtained:

(1) The Kriging model can effectively establish the high-precision nonlinear mathematical relationship between the selected 14 design variables and the optimization objectives with an R^2 value of 0.95356, which can meet the engineering needs.
(2) The hydraulic performance of the optimized model under design conditions and part-load conditions was greatly improved, the efficiency under design conditions was increased by 2.65%, and the head was increased by 0.83m under the premise that the power was relatively the same.
(3) The inner flow of the optimized model was significantly improved under the design condition, the large low-speed area and vortex area disappeared, and the pressure gradient change was reduced, which reduced the energy loss.

Author Contributions: Conceptualization, J.P. and W.W.; methodology, Z.H. and W.W.; software, Z.H. and W.W.; validation, C.H.; formal analysis, Z.H.; data curation, Z.H.; writing—original draft preparation, Z.H.; writing—review and editing, J.P. and W.W. All authors have read and agreed to the published version of the manuscript.

Funding: This research was funded by the Natural Science Foundation of Jiangsu Province (Grant No. 8 BK20190851), the Natural Science Foundation of China (Grant No. 51879121), and Primary Research & 9 Development Plan of Jiangsu Province (Grant No. BE2019009-1).

Conflicts of Interest: The authors declare no conflict of interest.

Nomenclature

Q_d (m^3/h)	Design flow rate
H (m)	Pump head
H (%)	Pump efficiency
n (r/min)	Rotational speed
n_s	Specific speed
Z_{im}	Number of impeller blades
Z_{di}	Number of diffuser vanes
D_j (mm)	Impeller inlet diameter
D_2 (mm)	Impeller outlet diameter
b_2 (mm)	Impeller outlet width
β_1 (degree)	Impeller inlet blade angle
β_2 (degree)	Impeller outlet blade angle
φ (degree)	Wrap angle of impeller blade
D_3 (mm)	Diffuser inlet diameter
D_4 (mm)	Diffuser outlet diameter
b_3 (mm)	Diffuser width
b_5 (mm)	Volute inlet width
D_5 (mm)	Volute base circle diameter
D_6 (mm)	Volute outlet diameter
T (N)	Impeller torque
Ω (rad/s)	Impeller angular velocity
ρ (kg/m^3)	Water density
p_{1tot} (Pa)	Total pressure at inlet of the pump
p_{2tot} (Pa)	Total pressure at outlet of the pump

References

1. Sakran, H.K.; Abdul Aziz, M.S.; Abdullah, M.Z.; Khor, C.Y. Effects of Blade Number on the Centrifugal Pump Performance: A Review. *Arab. J. Sci. Eng.* **2022**, 1–17. [CrossRef]
2. Arun Shankar, V.K.; Umashankar, S.; Paramasivam, S.; Hanigovszki, N. A Comprehensive Review on Energy Efficiency Enhancement Initiatives in Centrifugal Pumping System. *Appl. Energy* **2016**, *181*, 495–513. [CrossRef]
3. Liu, M.; Tan, L.; Cao, S. Performance Prediction and Geometry Optimization for Application of Pump as Turbine: A Review. *Front. Energy Res.* **2022**, *9*, 818118. [CrossRef]
4. Al-Obaidi, A.R. Influence of Guide Vanes on the Flow Fields and Performance of Axial Pump under Unsteady Flow Conditions: Numerical Study. *JMES* **2020**, *14*, 6570–6593. [CrossRef]
5. Bai, L.; Zhou, L.; Han, C.; Zhu, Y.; Shi, W. Numerical Study of Pressure Fluctuation and Unsteady Flow in a Centrifugal Pump. *Processes* **2019**, *7*, 354. [CrossRef]
6. Yang, J.; Pavesi, G.; Liu, X.; Xie, T.; Liu, J. Unsteady Flow Characteristics Regarding Hump Instability in the First Stage of a Multistage Pump-Turbine in Pump Mode. *Renew. Energy* **2018**, *127*, 377–385. [CrossRef]
7. Li, Z.; Zheng, X. Review of Design Optimization Methods for Turbomachinery Aerodynamics. *Prog. Aerosp. Sci.* **2017**, *93*, 1–23. [CrossRef]
8. Cho, S.; Kim, M.; Lyu, B.; Moon, I. Optimization of an Explosive Waste Incinerator via an Artificial Neural Network Surrogate Model. *Chem. Eng. J.* **2021**, *407*, 126659. [CrossRef]
9. Zhang, X.; Xie, F.; Ji, T.; Zhu, Z.; Zheng, Y. Multi-Fidelity Deep Neural Network Surrogate Model for Aerodynamic Shape Optimization. *Comput. Methods Appl. Mech. Eng.* **2021**, *373*, 113485. [CrossRef]
10. Keshtegar, B.; Mert, C.; Kisi, O. Comparison of Four Heuristic Regression Techniques in Solar Radiation Modeling: Kriging Method vs RSM, MARS and M5 Model Tree. *Renew. Sustain. Energy Rev.* **2018**, *81*, 330–341. [CrossRef]
11. Ren, C.; Aoues, Y.; Lemosse, D.; Souza De Cursi, E. Ensemble of Surrogates Combining Kriging and Artificial Neural Networks for Reliability Analysis with Local Goodness Measurement. *Struct. Saf.* **2022**, *96*, 102186. [CrossRef]
12. Hasanipanah, M.; Meng, D.; Keshtegar, B.; Trung, N.-T.; Thai, D.-K. Nonlinear Models Based on Enhanced Kriging Interpolation for Prediction of Rock Joint Shear Strength. *Neural Comput. Appl.* **2021**, *33*, 4205–4215. [CrossRef]
13. Tong, S.; Zhao, H.; Liu, H.; Yu, Y.; Li, J.; Cong, F. Multi-Objective Optimization of Multistage Centrifugal Pump Based on Surrogate Model. *J. Fluids Eng.* **2019**, *142*, 011101. [CrossRef]
14. De Donno, R.; Ghidoni, A.; Noventa, G.; Rebay, S. Shape Optimization of the ERCOFTAC Centrifugal Pump Impeller Using Open-Source Software. *Optim. Eng.* **2019**, *20*, 929–953. [CrossRef]

15. Ma, S.-B.; Kim, S.; Kim, J.-H. Optimization Design of a Two-Vane Pump for Wastewater Treatment Using Machine-Learning-Based Surrogate Modeling. *Processes* **2020**, *8*, 1170. [CrossRef]
16. Jaiswal, A.K.; Siddique, M.H.; Paul, A.R.; Samad, A. Surrogate-Based Design Optimization of a Centrifugal Pump Impeller. *Eng. Optim.* **2021**, 1–18. [CrossRef]
17. Chen, X.B.; Zhang, R.H.; Yang, W.F. Inverse Design and Optimization of Low Specific Speed Centrifugal Pump Blade Based on Adaptive POD Hybrid Model. *J. Appl. Fluid Mech.* **2022**, *15*, 453–464. [CrossRef]
18. Gan, X.; Pei, J.; Yuan, S.; Wang, W.; Tang, Y. Multi-Objective Optimization on Inlet Pipe of a Vertical Inline Pump Based on Genetic Algorithm and Artificial Neural Network. In Proceedings of the Volume 1: Flow Manipulation and Active Control; Bio-Inspired Fluid Mechanics; Boundary Layer and High-Speed Flows; Fluids Engineering Education; Transport Phenomena in Energy Conversion and Mixing; Turbulent Flows; Vortex Dynamics; DNS/LES and Hybrid RANS/LES Methods; Fluid Structure Interaction; Fluid Dynamics of Wind Energy; Bubble, Droplet, and Aerosol Dynamics, Montreal, QC, Canada, 15–20 July 2018; American Society of Mechanical Engineers: New York, NY, USA, 2018; p. V001T06A003.
19. Posa, A.; Lippolis, A. Effect of Working Conditions and Diffuser Setting Angle on Pressure Fluctuations within a Centrifugal Pump. *Int. J. Heat Fluid Flow* **2019**, *75*, 44–60. [CrossRef]
20. Yang, G.; Zhao, X.; Zhang, D.; Geng, L.; Yang, X.; Gao, X. Hydraulic Components' Matching Optimization Design and Entropy Production Analysis in a Large Vertical Centrifugal Pump. *J. Mech. Sci. Technol.* **2021**, *35*, 5033–5048. [CrossRef]
21. Lai, F.; Zhu, X.; Li, G.; Zhu, L.; Wang, F. Numerical Research on the Energy Loss of a Single-Stage Centrifugal Pump with Different Vaned Diffuser Outlet Diameters. *Energy Procedia* **2019**, *158*, 5523–5528. [CrossRef]
22. Wang, W.; Pei, J.; Yuan, S.; Yin, T. Experimental Investigation on Clocking Effect of Vaned Diffuser on Performance Characteristics and Pressure Pulsations in a Centrifugal Pump. *Exp. Therm. Fluid Sci.* **2018**, *90*, 286–298. [CrossRef]
23. Krige, D.G. A Statistical Approach to Some Basic Mine Valuation Problems on the Witwatersrand. *J. Chem. Metall. Min. Eng. Soc. S. Afr.* **1951**, *52*, 119–139.
24. Sacks, J.; Welch, W.J.; Mitchell, T.J.; Wynn, H.P. Design and Analysisi of Computer Experiments. *Stat. Sci.* **1989**, *4*, 409–423.